Chimney effect induced by smoldering fire in a U-shaped porous channel: A governing mechanism of the persistent underground coal fires

Zeyang Song[a,b,*], Xinyan Huang[c], Claudia Kuenzer[d], Hongqing Zhu[e], Juncheng Jiang[a,f,g], Xuhai Pan[a,f], Xiaoxing Zhong[b,*]

[a] *College of Safety Science and Engineering, Nanjing Tech University, 211816 Nanjing, PR China.*

[b] *Key Laboratory of Coal Methane and Fire Control, China University of Mining and Technology, 221116 Xuzhou, PR China.*

[c] *Department of Building Services Engineering, Hong Kong Polytechnic University, Hong Kong, PR China.*

[d] *Earth Observation Center, German Aerospace Center, 82234 Wessling, Germany.*

[e] *School of Emergency Management and Safety Engineering, China University of Mining and Technology, 100083 Beijing, PR China.*

[f] *Jiangsu Key Laboratory of Hazardous Chemicals Safety and Control, Nanjing Tech University, 211816 Nanjing, PR China.*

[g] *School of Environmental and Safety Engineering, Changzhou University, 213159 Changzhou, PR China*

Abstract

This paper presents underground coal fires (UCF) induced natural ventilation through a U-shaped porous channel. Height of the U-shaped channel (the fire depth) is one of key elements determining the accessibility of air supply to UCF. Conventionally, we acknowledge that under the external wind driving force, air supply to underground space should decay with increasing the fire depth. However, under the thermal buoyancy force induced by UCF, responses of air supply and UCF to the fire depth are uncertain. Herein we propose a 1/20-scale experimental framework to measure air velocity, and to quantify the burning rate, the fire spread rate and the burning temperature of UCF at different fire depths (H=1.6 - 4.6 m) with variable aperture sizes (Φ=1 - 4 cm). A one-dimensional model correlating the air velocity with the fire depth is validated and then extrapolates laboratory-scale free channels into field-scale (H=100 m) percolation channels. We find the 'chimney effect' – air supply driven by the buoyant smoke of UCF is unexpectedly enhanced with increasing the fire depth; the enhanced air supply due to the chimney effect facilitates burning of coal. The chimney effect, serving as a self-sustaining mechanism of air supply to UCF, is a significant governing mechanism for persistent UCF burning for hundreds or even thousands of years.

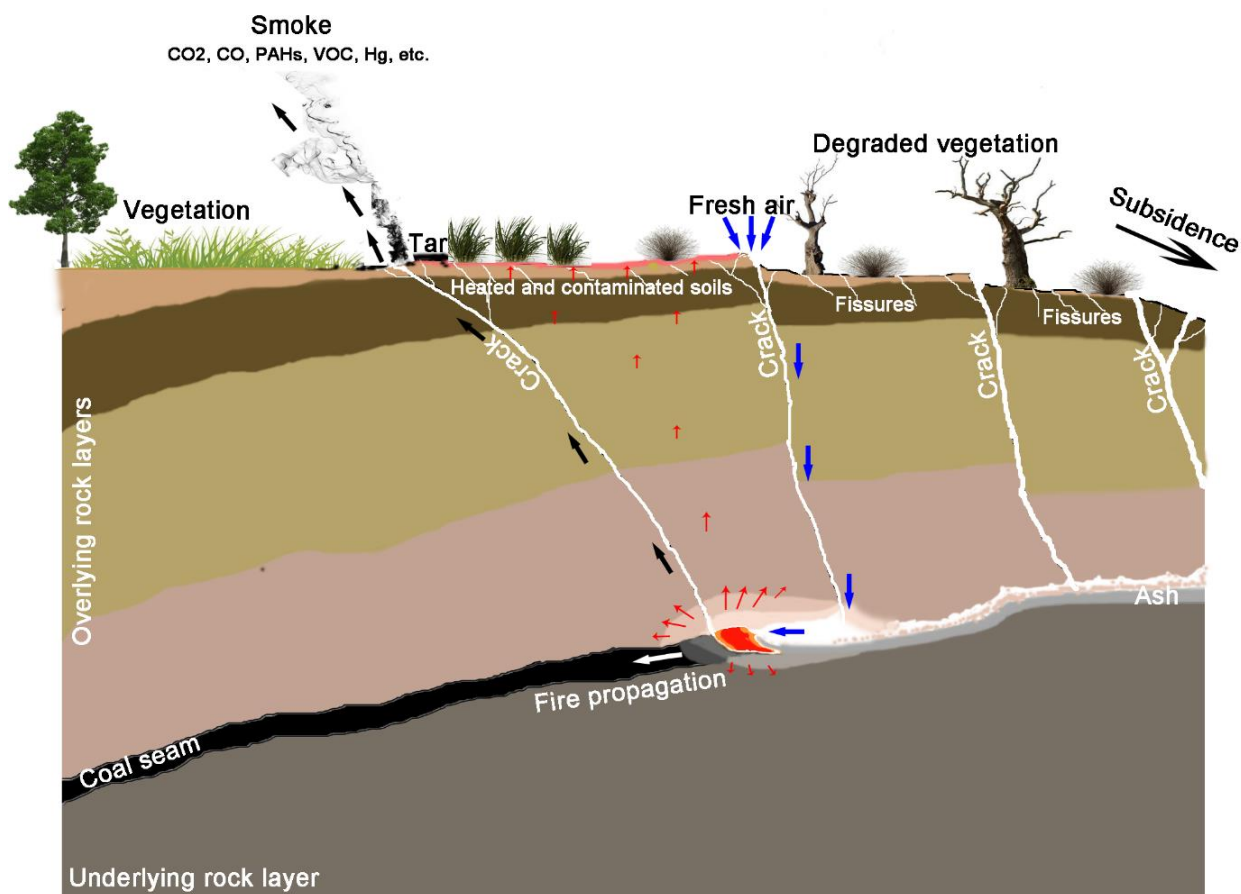**Keywords:** natural ventilation; thermal buoyancy; subsurface fire; stack effect

1. Introduction

Underground coal fires (UCF, see Fig. 1), referring to sites of slow combustion (smoldering) of subsurface coal, are an intractable hazard threatening the safety of coal mining industries and polluting the atmosphere and the lithosphere environments (Lu et al., 2018; Tang et al., 2019; Wang et al., 2018; Wang et al., 2016; Zhuo et al., 2019). UCF produce toxic products (CO (O'Keefe et al., 2010), tar (Engle et al., 2012), Polycyclic Aromatic Hydrocarbons (PAHs) (Liu et al., 2012), volatile organic compounds (VOCs) (Yan et al., 2015), Hg (Hower et al., 2009; O'Keefe et al., 2010), etc.), resulting in heavy air pollution and soil contamination. UCF release massive thermal energy, which is transferred to the ground surface (Wessling et al., 2008b) and results in severe vegetation degradation (Kuenzer et al., 2012; Kuenzer et al., 2007). UCF can also lead to geo-hazards such as collapse, subsidence, and landslides (Ide et al., 2010; Jiang et al., 2011; Kuenzer and Stracher, 2012). Additionally, UCF are a significant source of ancient carbon release from coal seams to the atmosphere. Understanding the role of greenhouse gas emissions (GHGs) emitted from UCF in the global climate change is still an emerging research topic (Engle et al., 2011; O'Keefe et al., 2010; Song et al., 2019a; van Dijk et al., 2011).

---

* Corresponding authors.
Email addresses: zeyang.song@njtech.edu.cn (Z. Song); xy.huang@polyu.edu.hk (X. Huang); zhxxcumt@163.com (X. Zhong).

Nomenclatures

a	stoichiometric coefficient of CO_2 production		formula of coal
A	area, m^2	Y	mass fraction, %
b	stoichiometric coefficient of CO production	z	oxygen atom number in molecular formula of coal
C	discharge coefficient		
g	gravitational acceleration, $m\,s^{-2}$		
H	fire depth, m	*Greek symbols*	
K	permeability, m^2	μ	dynamic viscosity, $kg\,m^{-1}\,s^{-1}$
L	height of coal bed, m	ρ	density, $kg\,m^{-3}$
ΔL	height difference, m	K	permeability, m^2
m	mass, g	Φ	aperture diameter, cm
$\dot{m}$	burning rate, $g\,s^{-1}\,m^{-2}$		
$\dot{m}'$	burning rate, $kg\,s^{-1}$	*Subscripts*	
$\Delta\dot{m}$	mass flow rates, $kg\,s^{-1}$	a	air, aperture area
M	molar mass, $g\,mol^{-1}$	am	ambient
$\overline{M}$	average molar mass, $g\,mol^{-1}$	b	burning area
ΔP	pressure drop, Pa	co	coal, coal seam
t	time, h	ch	percolation channel
T	temperature, °C	CO	carbon monoxide
U	fire spread rate, $cm\,h^{-1}$	CO_2	carbon dioxide
V	gas flow velocity, $m\,s^{-1}$	ex	exhaust gas
$\overline{V}$	average air velocity, $m\,s^{-1}$	F	fuel
x	carbon atom number in molecular formula of coal	k	thermocouple index
		max	maximum
X	gases volume concentrations, vol.%	O_2	oxygen
y	hydrogen atom number in molecular	p	peak
		pl	smoke
		S	fire spread

UCF can be ignited by the self-heating of coal oxidation (Liu et al., 2019; Song and Kuenzer, 2014; Yang and Qiu, 2019; Zhuo et al., 2019), wildland fires (Rein, 2013), lightning strike (Prakash et al., 2011), and mining activities (Kuenzer et al., 2012). They continue to burn underneath the Earth's surface with divers air supply through narrow channels (e.g., cracks, fractures, and fissures, see Fig. 1). UCF is one of the most persistent fires on the Earth, and can burn and smolder for hundreds or even thousands of years (Ellyett and Fleming, 1974). However, the mechanism of such persistence is still mysterious.

For the persistence of UCF, abundant fuel in a coal reservoir is a precondition; slow burning (propagation) rate of smoldering fire provides a beneficial condition (Rein, 2013). Once underground deposited coal is ignited, the persistence of UCF is determined by certain extinct conditions of smoldering fires, which are mainly associated with the heat and mass (air) transfer processes (Rein, 2013). Underground rocks/sediments perform fine thermal insulation conditions for UCF, but air in underground fractured or porous zones is very depleted. Thus, air supply is a crucial process governing the persistent UCF.

The natural driving forces of air supply to subsurface porous zones include wind, atmospheric pressure fluctuation (Song et al., 2015b), topographic effect (Song et al., 2014), and thermal buoyancy (Krevor et al., 2011; Li et al., 2018; Song et al., 2019b). Recently, it has demonstrated that thermal buoyancy is a significant force for air supply to UCF (Krevor et al., 2011; Li et al., 2018; Song et al., 2019b). For subsurface fires, the fire depth (H) is an important element determining the accessibility of air supply to UCF. Under different driving forces, the responses of the air flow to increasing the fire depth may behave differently. We acknowledge that under natural forces such as wind, topographic effect, and atmospheric pressure fluctuations, air supply to underground space should decay with increasing the depth. However, with thermal buoyancy generated by UCF itself (Krevor et al., 2011; Li et al., 2018; Song et al., 2019b), responses of the air supply and UCF to the fire depth are still uncertain.

Fig. 1. Schematic chart of UCF and their environmental impacts (Song et al., 2019b).

Thermal buoyancy driven natural convection is widely applied to improve air conditions in buildings (Lei et al., 2016) and to generate green energy, e.g., the solar chimney (Zamora and Kaiser, 2009; Zhou et al., 2009) and the channel-chimney system (Auletta et al., 2003; Nasri et al., 2015); on the other hand, it has destructive influences on, for instance, fire protection of buildings (Gao et al., 2017; Ji et al., 2017), the gas-cooled reactors (Chen et al., 2017), and underground coal reservoirs (Krevor et al., 2011; Li et al., 2018; Song et al., 2019b). It has demonstrated that geometrical configurations (Auletta et al., 2003; Nasri et al., 2015; Zamora and Kaiser, 2009; Zhou et al., 2009) and free/porous (Li et al., 2018; Sharma et al., 2018; Song et al., 2019b) media of the channel have crucial effects on the behaviors of the natural convection. For thermal buoyancy driven natural ventilation in a vertical free channel, the chimney effect (the stack effect) has been well recognized; gas flow induced by the chimney effect increases with increasing the height of the channel. Recently, we reported the characteristic behavior of thermal buoyancy driven air flow through thin porous media in a U-shaped channel (Song et al., 2019b). The chimney effect of such U-shaped configuration with porous media widely occurs in the fields of underground thermal engineering (Liu et al., 2018) as well as in the nature like underground coal fires (UCF) (Krevor et al., 2011; Li et al., 2018; Song et al., 2019b). But investigation on this topic has been paid rare attention (Sharma et al., 2018; Song et al., 2019b) and our understanding on its thermo- and fluid-dynamics is still poor. In this paper, we aim to characterize the dependences of the gas flow and the smoldering fire in a U-shaped porous channel on the channel's height, and then attempt to reveal the governing mechanism of persistent UCF.

Herein we develop a 1/20-scale laboratory experimental framework (see Fig. 2) to mimic buoyancy-driven UCF in the field (Song et al., 2019b) and unravel the relationship between UCF and the fire depth. In Section 2, the experimental setup and procedures are illustrated; approaches to quantify the burning rate and the fire spread rate are also detailed. Section 3 presents the dependences of the air supply, the burning rate, the fire spread rate and the maximum burning temperature on the fire depth. A one-dimensional model correlating the air supply and the fire depth, uncertain analyses on permeability and spatial scale, as well as the governing mechanism of persistent UCF are discussed in Section 4.
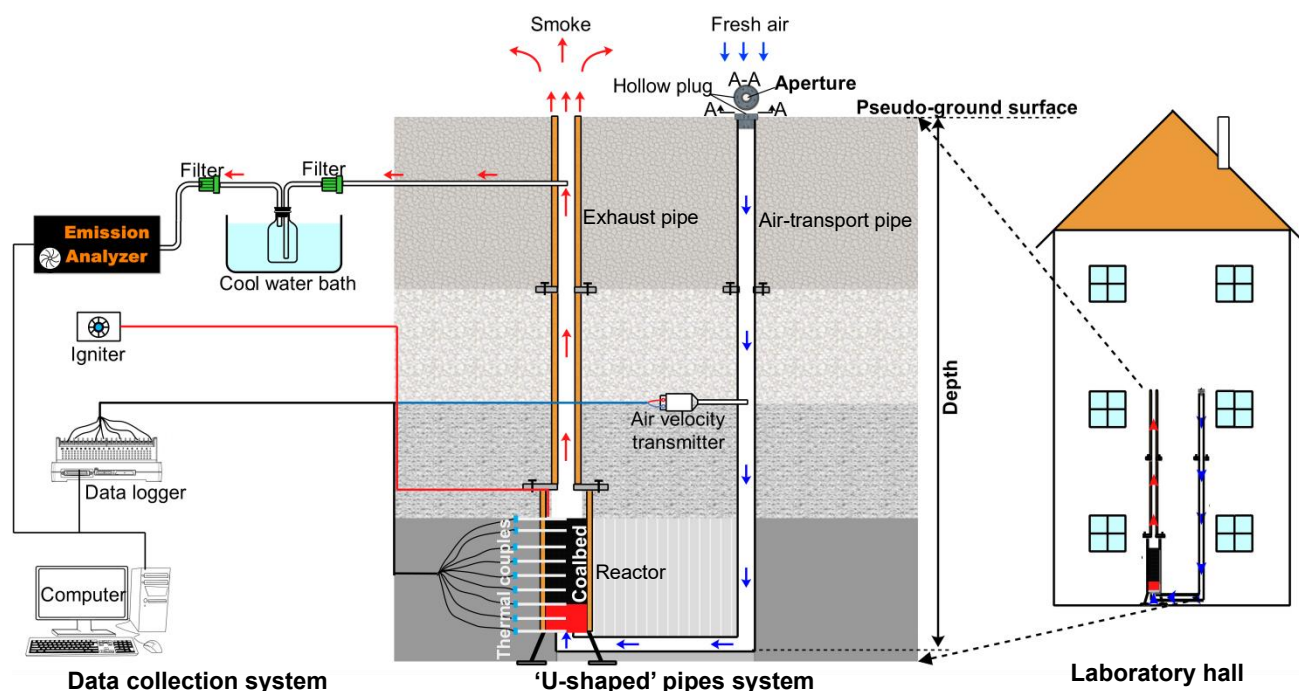
Fig. 2. Schematic diagram of the experimental setup and data collection system (Song et al., 2019b).

2. Experimental method

2.1. Experimental setup

In-situ UCF (see Fig. 1) is covered by complex geological rocks and propagates along multiple directions (three dimensions), which results in poor repeatability and controllability for experimental research. This work focuses on the chimney effect induced by UCF, in which the vertical direction is the most important. For the sake of simplicity, one-dimensional laboratory experiment framework was established (Song et al., 2019b).

A schematic diagram of experimental setup was shown in Fig. 2. The top surface of the 'U-shaped' structure was considered as the pseudo land surface. Then, space below the top surface was considered to be an underground (see Fig. 2). A vertical pipe with a diameter of 12 cm and length of 60 cm was employed as the combustion reactor to mimic the UCF. A vertical exhaust pipe and a 'L-shaped' inlet pipe were fitted at the top and bottom of the reactor, respectively. The diameter of both pipes was 6 cm. The vertical lengths of pipes were variable, which provides the first laboratory-scale experiment to simulate UCF and study its dependence on the fire depth. Hollow plugs with variable aperture sizes were inserted into the top 'L-shape' pipe to investigate the influence of the ventilation channel (e.g. crack) size. In the field, the fire depth is approximately 100 m (Shi et al., 2017) and the channel width ranges from several centimeters to hundreds of centimeters (Kuenzer and Stracher, 2012). The experimental framework allowed to vary fire depth (H=-1.6 m - 4.6 m) via adjusting the vertical lengths of transport pipes and aperture size (Φ=1 and 4 cm) via a hollow plug. Previous scale analysis demonstrated that the laboratory scale was representative for a 1/20 scale of UCF in the field (Song et al., 2019a; Song et al., 2019b). Alumina silicate wools with a thickness of 2 cm were attached inside the reactor and outside the exhaust pipe to mimic the thermally insulated environment of underground rock layers. A metal mesh (1.5 mm × 1.5 mm) was placed at the bottom of the reactor to hold coalbed and solid residuals. The coalbed was ignited by an electrical heater.

The airflow velocity (V_a) was measured at a fixed point in the centerline of the vertical pipe by the anemometer (FMA900R, OMEGA, USA; range: 0-1.02 m s^{-1}, accuracy: ±2% FS). A small portion of the exhaust gas flow (1 mL min^{-1}) was drawn by a pump from the exhaust pipe to the gas analyzer (TESTO 350, TESTO, Germany). Before entering the gas analyzer, the exhaust-gas sample was cooled through a water bath, and the contaminative products, such as tar-containing vapor and particle materials, were removed by filters. Gas volume fractions of O_2 (0-25%, ±0.2%), CO_2 (0-50%, ±0.3%), and CO (0-40%, ±4%) were measured. Multiple thermocouples (TCs) (inconel sheath Type K, OMEGA, USA) were inserted into the reactor with 2-cm vertical intervals and recorded the temperatures of coal and smoke.

Two sets of experiments with different heights of coalbed were conducted. Due to smaller flow resistance

through porous media, a thinner coalbed was considered as the first set of experiments in order to quantify the air velocity and the burning rate. However, the results showed that fire spread cannot be observed from the thin-coalbed experiments (see the temperature data published in the previous work (Song et al., 2019a; Song et al., 2019b)). Hence, thicker coalbed, i.e. the second set of experiments had to be taken into account for examining the dependence of fire spread on the fire depth and the aperture size.

(a)   A thin coalbed with a height of 14 cm and mass (m_{co}) of 595.70 ±1.10 g was filled into the reactor to study the responses of the air supply (V_a) and the burning rate ($\dot{m}_F$) to an increasing the fire depth. Six TCs (TC$_1$-TC$_6$) were inserted into the coalbed. The TC$_1$ and TC$_2$ measured the lower and upper boundaries of the burning zone, respectively. Herein, we chose the measurement of TC$_2$ as the characteristic burning temperature (T_2), considering TC$_1$ could be affected by the igniter. On the other hand, TC$_7$ was put closely above the top surface of the coalbed to monitor the smoke temperature (T_7).

(b)   A thick coalbed with a height of 28 cm (m_{co}=1156.80±37.60 g) was piled up to investigate the response of the fire spread rate (U_s) and the maximum burning temperature (T_{max}) to the rise of the fire depth. Thirteen TCs (TC$_{1-13}$) were inserted into the coalbed. U_s and T_{max} were obtained from the temperature history data (see Fig. 5).

2.2. Experimental procedure

Step I: preparing of the sample. High-volatile bituminous coal that is highly susceptible to spontaneous combustion (Song et al., 2017a; Song et al., 2017b) was chosen in the experiments. Chunks of fresh coal samples were collected from the Chang Cun Coal Mine in Henan Province, P.R. China. Sampling procedures were referred to the Chinese standard GB/T19494.1-2004. They were immediately stored into air-proof plastic buckets. Before the experiment, large coal samples were crushed in the ambient and sieved manually into small coal particles with a diameter of 7 ± 2 mm. The proximate and ultimate analyses were conducted (Song et al., 2017a; Song et al., 2017b) according to GB/T212-2008 (moisture, ash, and volatile contents), GB/T476-2008 (carbon (C) and hydrogen (H)), GB/T214-2007 (sulfur (S)), and GB/T19227-2008 (nitrogen (N)). Bulk density, porosity and permeability of coalbed were measured. Properties of the sample were shown in Table 1.

Table 1. Properties of coal sample.

Basic properties		Value
Proximate analysis (dry base, wt.%)	Moisture	2.86
	Volatile	34.75
	Ash	14.84
	Fixed carbon	47.55
Ultimate analysis (%, Dry ash-free basis)	Carbon	71.104
	Hydrogen	5.438
	Oxygen	21.880
	Nitrogen	1.313
	Sulfur	0.265
Density (kg m^{-3})		1589.6 ± 9.420
Bulk density (kg m^{-3})		667.04 ± 28.85
Porosity (%)		54.98 ± 1.95
Permeability (m^2)		4.23×10^{-7}

Step II: apparatus installation. The metal mesh and the igniter were placed at the bottom of the reactor. The thermal insulation was attached to the inner wall of the reactor. Coal particles were slowly filled into the reactor to ensure the homogeneity. Gas transport pipes were connected to the reactor. Under an air-tight condition, TCs, air velocity sensor, and the exhaust gas sampling tube were inserted into the reactor, air-transport pipe, and exhaust pipe, respectively. The TCs and the anemometer were linked to the data logger. The sampling tube of exhaust gas was successively connected to the water bath, the filter, and the gas analyzer. Both the data logger and the gas analyzer were connected to a computer to record data.

Step III: initializing UCF. The igniter was turned on to heat the coal sample and initiate a warm smoke. The igniter was automatically turned off when the ignition temperature was reached. To ensure a successful ignition, the ignition temperature was set to the peak temperature (T_p) of the self-sustaining coal fire (see Fig. 5). Once ignited, the air infiltration driven by the buoyant smoke was sufficient for feeding coal smoldering combustion.

Step IV: measuring parameters. Since ignition, V_a, T, and $X_{ex,i}$ (species i=O_2, CO_2, and CO) were simultaneously recorded every 2 s and saved on the computer. The experiment was terminated when V_a=0 cm s^{-1} and $X_{ex,CO2}$=0.

Each experiment was repeated by two times. All experiments were conducted inside a large-space laboratory hall to eliminate external wind.

2.3. Estimating burning rate

The burning rate ($\dot{m}_F$) is defined as the burnt coal mass per unit time and unit burning area. Strictly speaking, gaseous products of UCF include H_2O, CO_2, CO, and unburnt hydrocarbons (C_mH_n). In the exhaust gas, mass fractions of CO_2 (Y_{CO2}) and CO (Y_{CO}) are far larger than C_mH_n (Y_{CmHn}). Hence, we assume that C_mH_n in exhaust gas is ignorable. Coal combustion of UCF is simplified into a global one-step oxidation reaction:

$$C_xH_yO_z + \left(\frac{y}{4} + a + \frac{b}{2} - \frac{z}{2}\right)O_2 \rightarrow aCO_2 + bCO + \frac{y}{2}H_2O \tag{1}$$
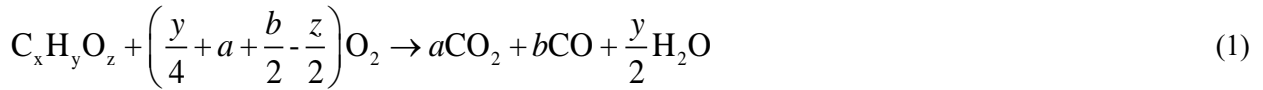
According to the ultimate analysis in Table 1, x, y and z in Eq. (1) are equal to 4.33, 3.98, and 1, respectively. According to the mass conservation, we have

$$a + b = x \tag{2}$$

Besides,

$$\frac{a}{b} = \frac{X_{ex,CO_2}}{X_{ex,CO}} \tag{3}$$

Then, a and b can be written as

$$a = \frac{x}{1 + \dfrac{X_{ex,CO}}{X_{ex,CO_2}}} = x\eta \tag{4}$$

$$b = \frac{x}{1 + \dfrac{X_{ex,CO_2}}{X_{ex,CO}}} \tag{5}$$

where η is the combustion efficiency (Yokelson et al., 1996) that is defined as

$$\eta = \frac{X_{ex,CO_2}}{X_{ex,CO_2} + X_{ex,CO}} \tag{6}$$

According to Eq. (1), we have

$$\Delta\dot{m}_{O_2} = \left(\frac{y}{4} + a + \frac{b}{2} - \frac{z}{2}\right)\frac{32}{(12x + y + 16z)}\dot{m}_F' \tag{7}$$

$$\Delta\dot{m}_{CO_2} = a\frac{44}{(12x + y + 16z)}\dot{m}_F' \tag{8}$$

They can also be expressed as:

$$\Delta\dot{m}_{O_2} = \dot{m}_{a,O_2} - \dot{m}_{ex,O_2} = \left(\rho_a V_a A_a\right)Y_{a,O_2} - \left(\rho_{ex}V_{ex}A_{ex}\right)\frac{M_{O_2}}{M_{ex}}X_{ex,O_2} \tag{9}$$

$$\Delta\dot{m}_{CO_2} = \left(\rho_{ex}V_{ex}A_{ex}\right)Y_{ex,CO_2} = \left(\rho_{ex}V_{ex}A_{ex}\right)\frac{M_{CO_2}}{M_{ex}}X_{ex,CO_2} \tag{10}$$

Combining Eq. (2), Eqs. (7) - (10), we have

$$\dot{m}_F = \frac{1000\dot{m}_F'}{A_b} = \frac{2090\rho_a A_a V_a}{A_b(10.64 + 8.66\eta + 17.32\eta \frac{X_{ex,O_2}}{X_{ex,CO_2}})} \tag{11}$$

In Eq. (11), we have ρ_a=1.29 kg m^{-3}, $A_a/A_b = \Phi^2/64$. Note that Φ is the aperture diameter in cm. Finally, the burning rate is expressed as

$$\dot{m}_F = \frac{42.13\Phi^2 V_a}{10.64 + 8.66\eta + 17.32\eta \frac{X_{ex,O_2}}{X_{ex,CO_2}}} \tag{12}$$

2.4. Estimating fire spread rate

The local fire spread rate ($U_{s,k}$) can be estimated from the time lapse ($\Delta t_k = t_{k+1} - t_k$) of the fire front arrival (i.e., temperature peaks, T_p) at two consecutive TCs (TC$_k$ and TC$_{k+1}$) and the distance (ΔL) between them (Pironi et al., 2011):

$$U_{s,k} = \frac{\Delta L}{\Delta t_k} \tag{13}$$

In this study, ΔL equals to 2 cm. The average fire spread rate (U_s) crossing the whole coal column was calculated based on $U_{s,k}$.

3. Experimental results

3.1. Chimney effect

Dragged by the buoyant smoke in the exhaust pipe, fresh air flows downward to the coalbed (Krevor et al., 2011; Song et al., 2019b). The evolution of air velocity (V_a) with the smoke temperature (T_7) and the fire depth (H=1.6-4.6 m) is presented in Fig. 3. The air velocity increases with increasing either the smoke temperature or the fire depth. Such enhancement of the air supply results from the stronger buoyancy, that is, the chimney effect of UCF.

Air flow through a thermally decomposed thin porous media is controlled by the thermosolutal buoyancy and the porous structure of coalbed (Song et al., 2019b). Fig. 3a illustrates two distinct stages of the air velocity against the smoke temperature. At the *Stage I*, the thermal buoyancy is weak but the porous coalbed is stable and thick (Song et al., 2019b). In this case, the air velocity is small and has a weak dependence on the smoke temperature and the fire depth. At the *Stage II*, the porous coalbed is decomposed due to smoldering combustion, facilitating natural ventilation (Song et al., 2019b). Thus, an abrupt increase of air velocity takes place. At this stage, air supply is more sensitive to the rise of the burning temperature and the fire depth.

The phenomenon that air velocity induced by smoldering coal fires with 1.6 m depth starts to increase when smoke temperature reaches to 450°C (see Fig. 3(a)) is mainly attributed to (a) the 'weaker chimney effect' and (b) the decomposition (pyrolysis) of porous media.

(a) With the same thermal buoyancy (smoke temperature), the air velocity induced by smoldering coal fire at a shallower depth is expected to be smaller. While the fire depth is 1.6 m and the smoke temperature is less than ~450°C, air velocity is so small that it is not measurable by the anemometer.

(b) Thermogravimetric (TG) analysis of pyrolysis (N$_2$ atmosphere) at slow heating rates (similar to the heat transfer scenario of smoldering combustion) for single large coal particle (7 ± 2 mm) was conducted. DTG data (not presented in paper) shows that the pyrolysis of coal focuses on ~450°C. The previous work (Song et al., 2019b) revealed that the permeability is improved and the flow resistance is decreased due to the shrunk coalbed, resulting from the fact that hot smoke (~450°C) transported upward benefits the pyrolysis of upper coal layers. At this circumstance, air velocity must be enhanced. Therefore, with the fire depth of 1.6 m, the air velocity starts to abruptly increase at ~450°C shown in Fig. 3(a). The mechanism in terms of couplings of thermal buoyancy and solid decomposition is detailed in the previous work (Song et al., 2019b).
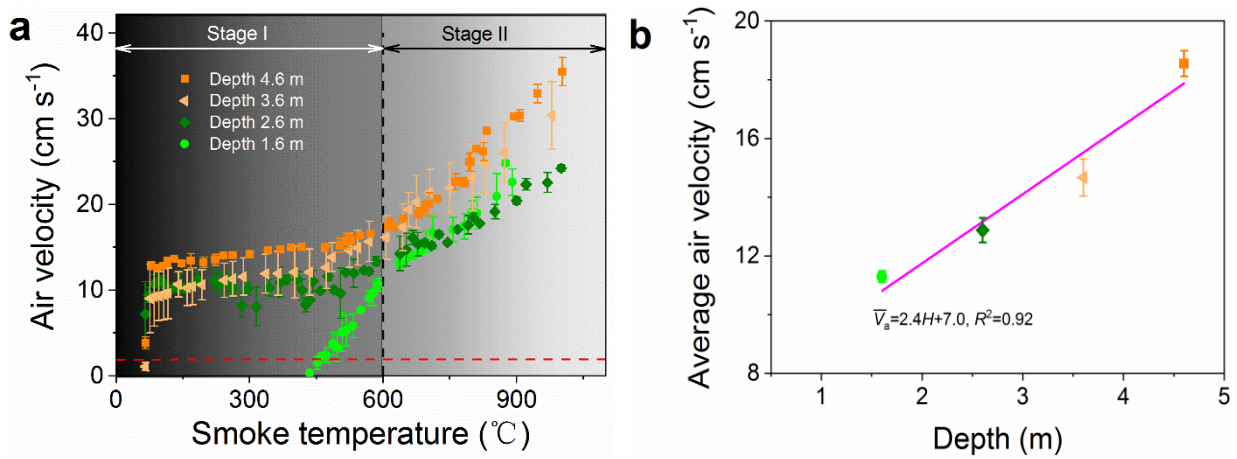
Fig. 3. Chimney effect of UCF. Plots of (a) the air velocity (V_a) with smoke temperature, and (b) average air velocity ($\bar{V}_a$) with fire depth (H) for UCF experiments with Φ= 4 cm. Error bars are standard deviations of replicated results.

3.2. Burning rate

In UCF experiments, the burning of coal is dominated by smoldering combustion ($\bar{\eta} \approx 0.6$, see Fig. 7). For the first time, the transient burning rate is estimated, as shown in Fig. 4. Generally, the burning rate slowly increases with increasing the burning temperature at the *Stage I* ($T_2 < \sim 1100$ °C). It is followed by a rapid increase in the burning rate ($T_2 < \sim 1100$ °C), resulting from the significant improvement of air supply at the *Stage II*.

Fundamentally, the burning rate of UCF is controlled by the air supply (discussed in Section 4.2). It is usually expected that a deeper UCF should burn at a slower rate or even be suppressed naturally. However, the experimental results indicate that with UCF generated the thermal buoyancy, the burning rate accelerates with increasing the fire depth due to the enhanced air supply. This result indicates that deeper UCF may burn faster in the field (see Discussion section).
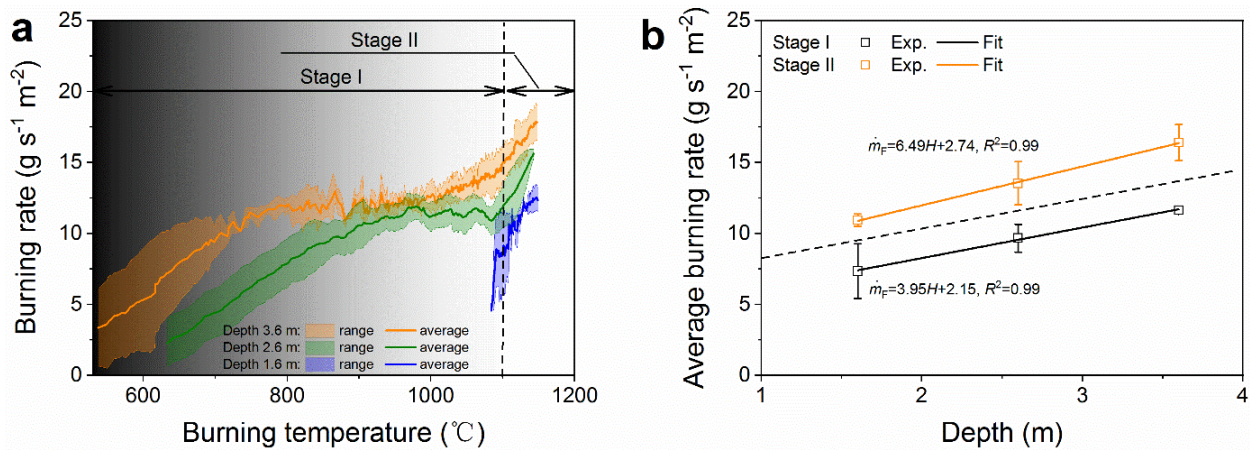
Fig. 4. Dependence of the burning rate on the fire depth. Plots of (a) the burning rate ($\dot{m}_F$) with the burning temperature, and (b) the average burning rate ($\dot{m}_F$) with the fire depth (H) for UCF experiments with Φ=4 cm. Error bars are standard deviations of repeated results.

3.3. Fire spread rate

Thirteen TCs' temperature history data from the second set (thick coalbed) of experiments is presented in Fig. 5. The successive peaks ($T_{peak,i}$) of TCs indicate that fire spreads upward (Huang and Rein, 2017; Pironi et al., 2011; Pironi et al., 2009). Those non-successive peaks suggest that the top surface of the coalbed is sinking under the gravity (Yang and Chen, 2018). If H increases from 1.6 m to 4.6 m, the burning time deceases from 13 h to 4 h for Φ=4 cm, and from 22 h to 12 h for Φ=1 cm. The temperature history data indicates that the fire spread (U_s) and the released thermal energy (T_{max}) are enhanced with increasing either H or Φ.

8

Fire spread rates (U_s) estimated by Eq. (13) are presented in Fig. 6a. In this work, the spread rate of UCF ranges between 0.4 and 2.5 cm h^{-1}, in accordance with ground smoldering coal fires (0.66±1.80 cm h^{-1}) (Hadden and Rein, 2011) and peat fires (0.50-2.00 cm h^{-1}) (Huang and Rein, 2017).
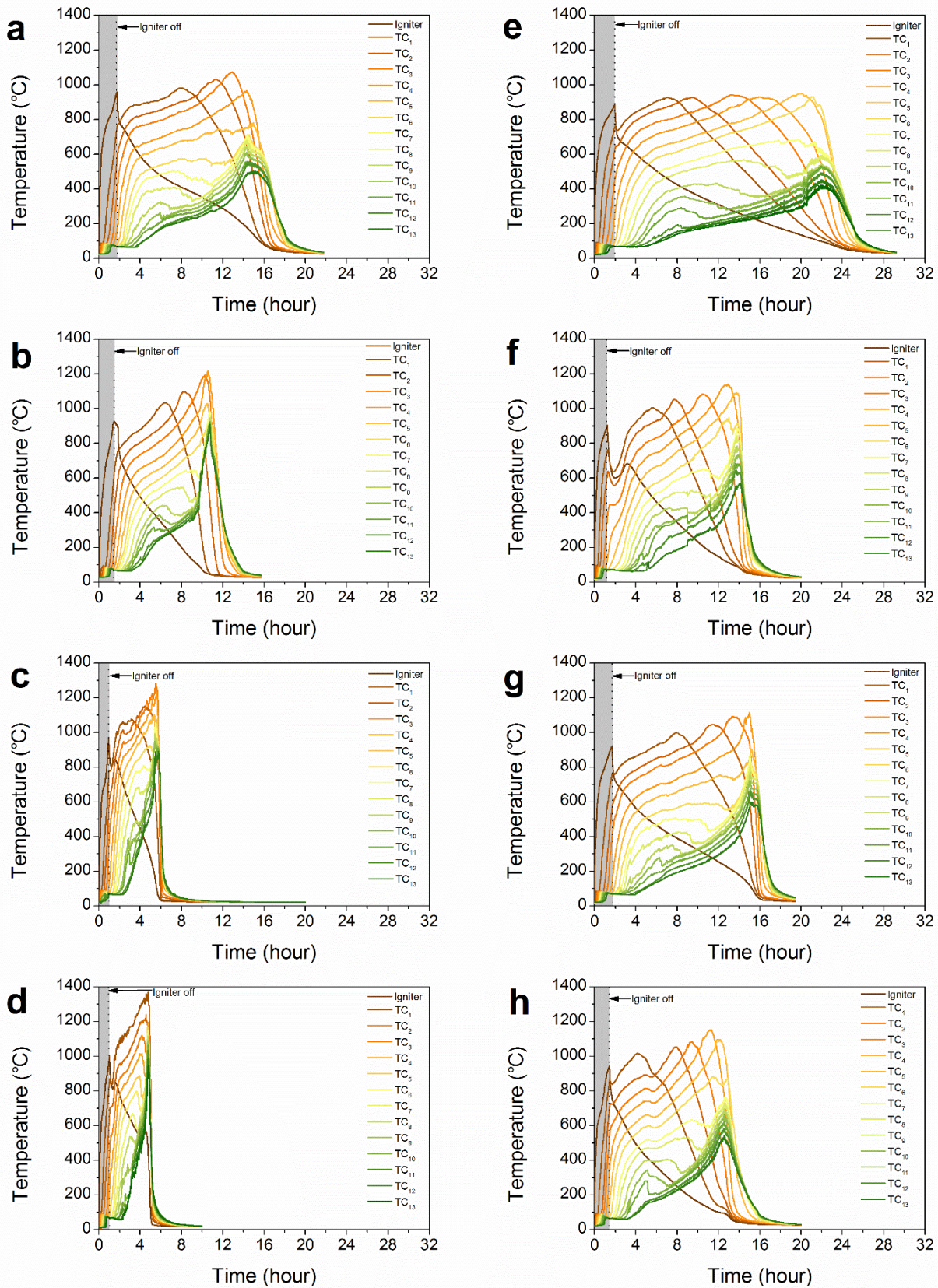
Fig. 5. TCs' temperature history data. Left column ((a)-(d)): Φ=4 cm; right column ((e)-(h)): Φ=1 cm. Four rows from the top to the bottom: (a) and (e), H=1.6 m; (b) and (f), H=2.6 m; (c) and (g), H=3.6 m; (d) and (h), H=4.6 m.

Aperture size, acting as the opening area of the ventilation channel, significantly impacts the fire spread rate. As shown in Fig. 6a, the fire spread rate is reduced by ~0.45 cm h^{-1} if the aperture size decreases from 4 cm to 1 cm. As can be seen in Fig. 6a, U_s increases with increasing the fire depth, even at the harsh condition of ventilation with a tiny aperture (Φ=1 cm). This result agrees well with the dependence of the burning rate on the fire depth (see Fig. 6b), because, fundamentally, the propagation of UCF is a result of the burning consumption of coal ($U_s = \dot{m}_F \rho_F$).
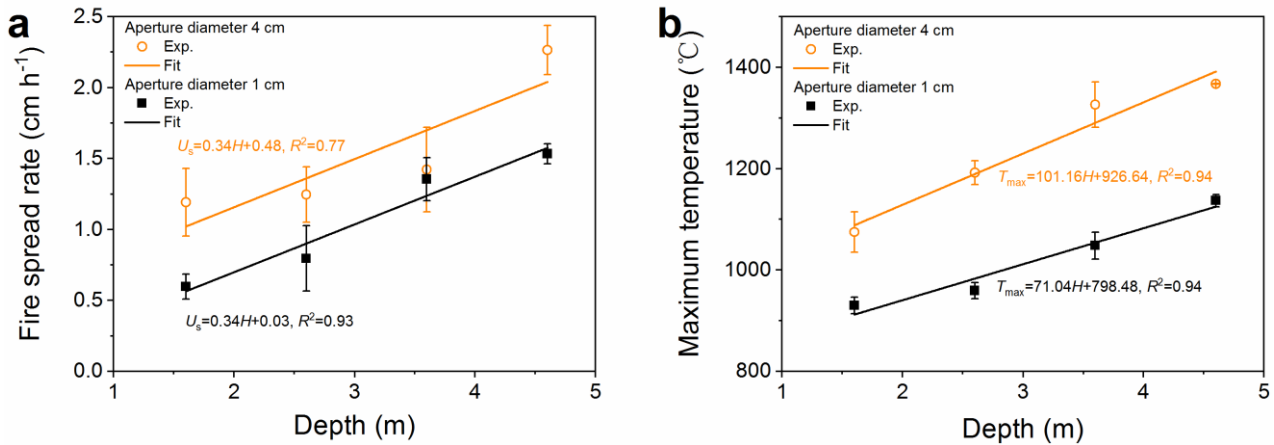
Fig. 6. Dependence of the fire spread rate and the maximum burning temperature on the fire depth. Plots of (a) the fire spread rate (U_s), and (b) the maximum burning temperature (T_{max}) against the fire depth (H). Error bars are standard deviations of repeated results.

3.4. Maximum burning temperature

Several temperature peaks (T_p) are observed in Fig. 5, which can be representative for the intensity of local coal burning effect. Herein, the maximum burning temperatures (T_{max}=max(T_p)) are considered to characterize the thermal response of UCF to the rising of the fire depth. T_{max} of UCF at different depths are plotted in Fig. 6b. T_{max} ranges between 900 °C and 1,400 °C, which is consistent with the measurements in the field (Song et al., 2015a; Zhang and Kuenzer, 2007) and the observations based on paralava and clinker (Grapes et al., 2009; Simmons et al., 1989).

Under air deplete condition, enhanced air supply is beneficial for char oxidation and increasing the burning temperature. Thus, it is expected that T_{max} increases with an increase of aperture size. As shown in Fig. 6b, T_{max} of UCF with Φ=4 cm is almost 200 °C higher than that with Φ=1 cm. Importantly, because of the enhanced air supply to deeper UCF induced by the chimney effect, T_{max} increases with increasing the fire depth (R^2=0.94). This result indicates that it is possible for deep UCF to release considerable thermal energy.

4. Discussion

4.1 Comparisons of chimney effects induced by smoldering fire in a U-shaped channel and by flaming fire in a vertical channel

The above results indicate that an increase of the fire depth can unexpectedly facilitate UCF (see Figs. 3 and 4). Such an unusual behavior is attributed to the chimney effect induced by smoldering fire in a U-shaped porous channel (see Fig. 3). The correlations of air velocity with the smoke temperature and the fire depth have been presented in the previous work (Song et al., 2019b). For the conventional chimney effect of vertical free channel e.g., building fires, a strong dependence on the building height (h) ($V_a \propto h^{1/3}$) exists (Gao et al., 2017; Shi et al., 2014). Comparatively, for the chimney effect of UCF, its dependence on the fire depth (H) is relatively weaker ($V_a \propto H^{0.018-0.330}$, see Ref. (Song et al., 2019b)). This weaker dependence is mainly attributed to large airflow resistance caused by porous coalbed. It implies that low permeability of percolation channels (Huang et al., 2001; Wessling et al., 2008a; Wolf and Bruining, 2007) in the field could be an uncertain factor limiting enhancement of air supply due to the chimney effect. Thus, a one-dimensional model is developed in the following 4.3 section to extrapolate the chimney effect of UCF from the laboratory-scale free

channels ('U-shaped' pipes, H=1.6-4.6 m) to field-scale percolation channels (H=0.1-100 m (Shi et al., 2017)).

4.2 Burning rate controlled by air supply

Eq. (12) indicates that the burning rate ($\dot{m}_F$) of UCF is associated with the air supply (V_a), the Graham's ratio ($X_{ex,CO_2}/X_{ex,O_2}$) (Singh et al., 2007) and the combustion efficiency (η). As can be seen in Fig. 7c, $\overline{\eta}$ is approximately 0.6, and almost independent on Φ and H. Then, we can consider $\overline{\eta}$ as a constant in this work. According to Eq. (12), then we have

$$\dot{m}_F \propto V_a, \quad X_{ex,CO_2}/X_{ex,O_2} \tag{14}$$
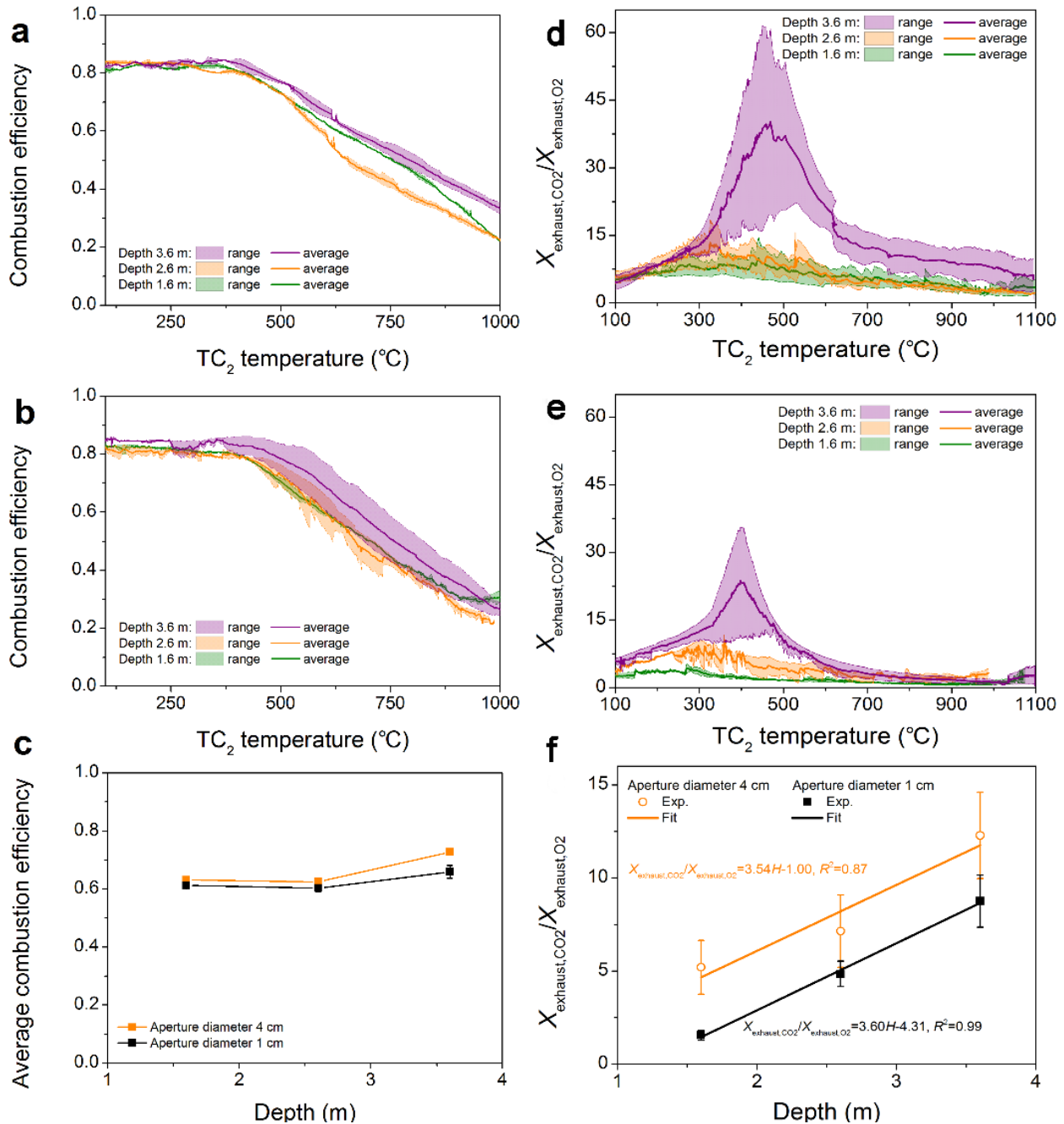
Fig.7. Dependence of the combustion efficiency and the Graham's ratio on the fire depth and the aperture size. (a)-(c) the combustion efficiency (η), and (d)-(f) the Graham's ratio. (a) and (d), Φ=4 cm. (b) and (e): Φ=1 cm. Error bars are standard derivations of replicate results.

Figure 7d-f shows that the Graham's ratio increases with either H (R^2=0.87 - 0.99) or Φ. In fact, with increasing the air supply, UCF will consume more oxygen (O_2) (lower X_{ex,O_2} in exhaust gas) and produce higher

$X_{ex,CO2}$, resulting in larger $X_{ex,CO_2}/X_{ex,O_2}$. Thus,

$$X_{ex,CO_2}/X_{ex,O_2} \propto V_a \tag{15}$$

Combining Eqs. (14) and (15), we can obtain

$$\dot{m}_F \propto V_a \tag{16}$$

Overall, the burning rate is fundamentally controlled by the air supply.

4.3 Extrapolating to the chimney effect induced by field-scale UCF in a U-shaped percolation channel

Laboratory experiments are limited to the small scale and the free channel (except for thin coalbed). Herein, a one-dimensional steady-state model is developed to extrapolate from the laboratory scale (H=1.6 - 4.6 m) to the field scale (up to 100 m), and more importantly from the free channels to the percolation channels (extreme harsh condition of ventilation). As discussed above, the burning rate of UCF is controlled by the air supply. Thus, in this model, the dependence of the air supply on the fire depth is emphasized and chemical kinetics of coal smoldering combustion is neglected. Previous work (Song et al., 2019b) suggested that the thermal buoyancy plays a leading role in the natural ventilation for UCF and the relationship between the fire depth and the solutal buoyancy is hardly quantified. Hence, the solutal buoyancy is excluded in this model. Besides, the air flow in the channel is laminar flow. For the sake of simplification, we ignore the flow resistance along the channel wall.

According to the Darcy's law and the Boussinesq approximation, in the vertical direction, we have

$$\Delta P = \int_{-H}^{0} \rho g (1 - \frac{T_{am}}{T_{pl}}) dH + \int_{0}^{2H} -\frac{\mu V_a}{K} dH \tag{17}$$

In Eq. (17), the first term at the right-hand side denotes the pressure drop induced by the thermal buoyancy. The second term represents the pressure drop due to the Darcy's flow in porous media. As for percolation channels, gas flow along the whole ventilation pathway ($2H$) obeys the Darcy's law. Note that the fire depth H is defined as the sum of the length of percolation channel and the height (L) of coal seam. Herein, we assume that porosity of percolation channels and coal seam is isotropic and then their permeability is K_{ch}. However, as for free channel, Darcy's flow is confined to the coal seam. Its permeability is K_{co}. Eq. (17) can be further developed to the following correlations:

For free channel:

$$\Delta P = \rho g (1 - \frac{T_{am}}{T_{pl}}) H - \frac{\mu V_a L}{K_{co}} \tag{18}$$

For percolation channel:

$$\Delta P = \rho g (1 - \frac{T_{am}}{T_{pl}}) H - \frac{2\mu V_a H}{K_{ch}} \tag{19}$$

Driven by the pressure drop ΔP, the velocity of air through an aperture can be expressed as (Linden, 2003):

$$V_a = C \sqrt{2 \frac{\Delta P}{\rho}} \tag{20}$$

Substitute Eq. (18) and Eq. (19) into Eq. (20), we can obtain that
for free channel:

$$V_a = C \sqrt{2gH(1 - \frac{T_{am}}{T_{pl}}) + \frac{2L^2\mu^2 C^2}{\rho^2 K_{co}^2} - \frac{L\mu C^2}{\rho K_{co}}} \tag{21}$$

for percolation channel:

$$V_a = C \sqrt{2gH(1 - \frac{T_{am}}{T_{pl}}) + \frac{4H^2\mu^2 C^2}{\rho^2 K_{ch}^2} - \frac{2H\mu C^2}{\rho K_{ch}}} \tag{22}$$

Based on Eqs. (21) and (22) with C=0.035, T_{pl}=600 °C, and T_{am}=27 °C, dependence of the air supply (V_a) on the fire depth (H) within a range of permeability (K_{co}=10^{-8}-10^{-6} m², K_{ch}=10^{-7}-10^{-6} m²) (Wessling et al., 2008a; Wolf and Bruining, 2007) is presented in Fig. 8. Sensitivity analyses of K, C, T_{pl}, and T_{am} are shown in Fig. 9.
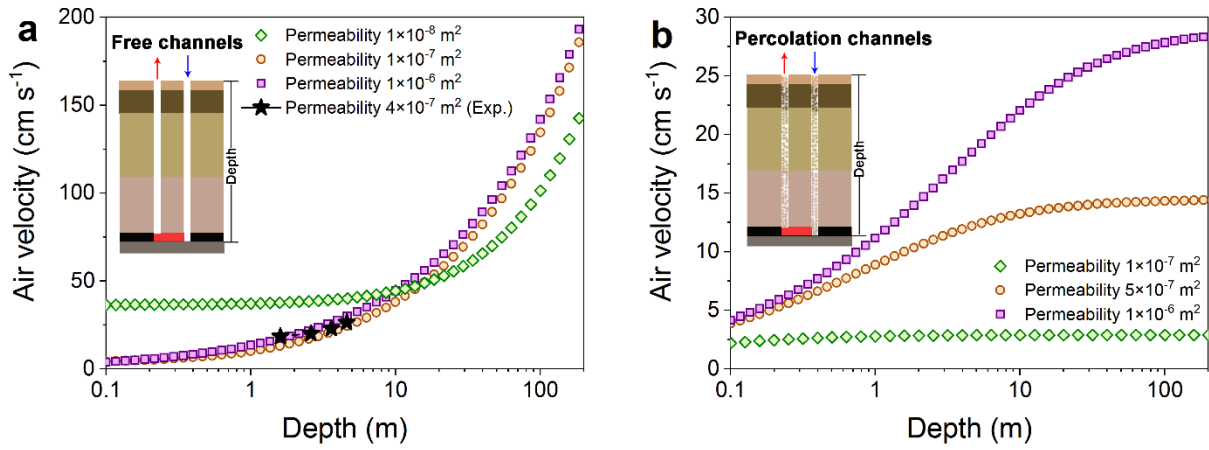
Fig. 8. Response of the air supply to increasing the fire depth: (a) free channels, and (b) percolation channels.

Figure 8a shows that analytical results of shallow UCF in free channels agree well with experimental results. It is expected that, as can be seen in Fig. 8, the chimney effect of UCF with percolation channels is weaker than with free channel. Importantly, the model confirms that the air supply is enhanced with increasing the fire depth up to >100 m even though air transports through percolation channel. However, the chimney effect of UCF in percolation channel is very sensitive to the permeability. The chimney effect almost disappears if the permeability of percolation channel is less than 10^{-7} m^2 (see Fig. 8b), which is in accordance with numerical simulations of UCF (Wolf and Bruining, 2007) and laboratory experiments of thermal convective venting in soils (Ganot et al., 2014). This result provides a valuable reference information for the fire-fighting engineering to control the critical permeability of loess covered at ground surface and injected inside ventilation channel (Song and Kuenzer, 2014).
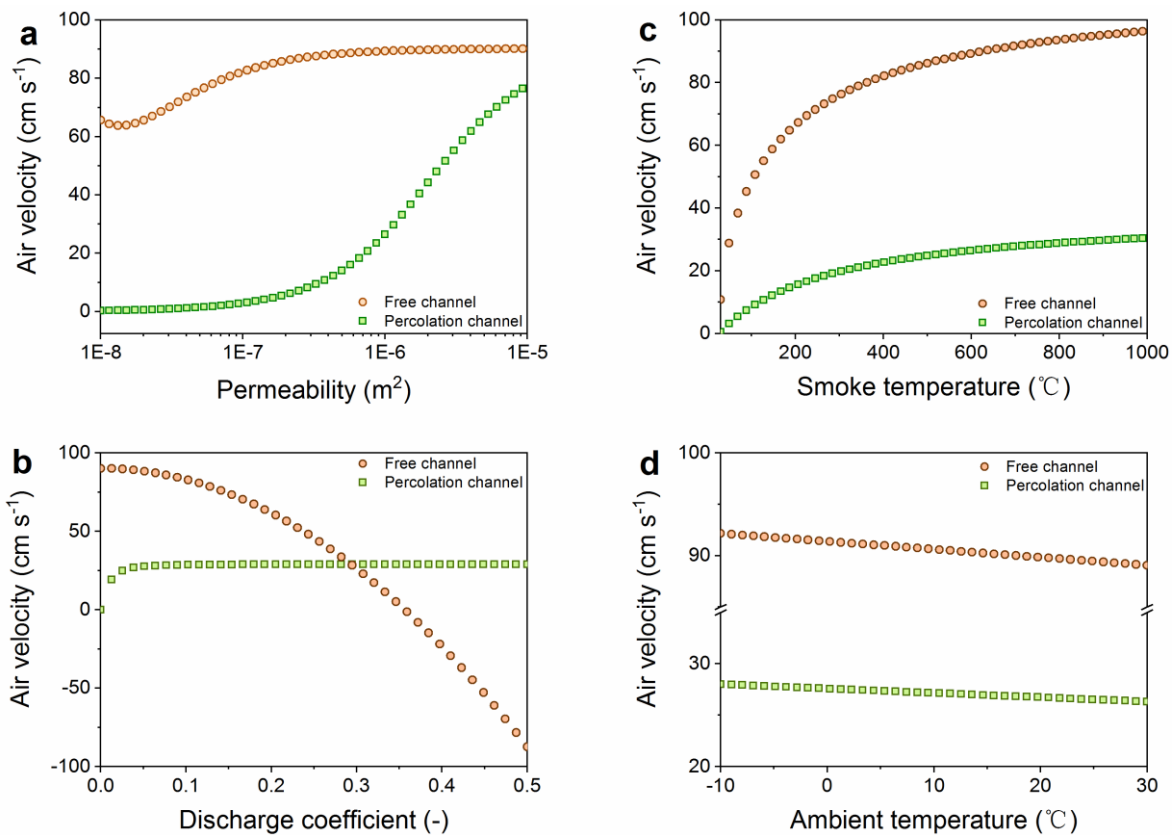
Fig. 9. Sensitive analyses of parameters in the extrapolating model. (a) the permeability (H=40 m, C=0.035, T_{pl}=600 ℃, and T_{am}=27 ℃), (b) the discharge coefficient (H=40 m, K_{co} (K_{ch})=10^{-6} m^2, T_{pl}=600 ℃, and T_{am}=27 ℃), (c) the smoke temperature (H=40 m, K_{co} (K_{ch})=10^{-6} m^2, C=0.035, and T_{am}=27 ℃), and (d) the ambient temperature (H=40 m, K_{co} (K_{ch})=10^{-6} m^2, C=0.035, and T_{pl}=600 ℃).

A wide range sensitivity analyses of the permeability, the discharge coefficient, the smoke temperature, and the ambient temperature are illustrated in Fig. 9. For free channel, the air velocity is very sensitive to the discharge coefficient and the smoke temperature; for percolation channel, it is sensitive to the permeability and the smoke temperature. The ambient temperature varying from -10 °C to 30 °C has limited influence on the air velocity for both free channels and percolation channels. The sensitivity analyses also indicate that for free channels the air velocity could be overestimated if $K_{co} < \sim 10^{-8}$ m^2 (see Fig. 8a), and underestimated if $C > 0.25$.

4.4 Governing mechanism of the persistent UCF

In practice, free channels may intersect with percolation channels. Air supply to UCF in the field could be improved by multiple air-transport channels, comparing to the single channel considered in the model. In addition, the model excludes the heat dissipation and the dynamic couplings of hydraulic and thermal processes: a deeper UCF dissipates less heat to the ambient (Huang et al., 2001; Wolf and Bruining, 2007); enhancement of air supply results in higher burning temperature and stronger thermal buoyancy, which in turn enhances air supply further. Thus, the chimney effect of UCF in the field is likely more dominant than that presented in Fig. 8b. The experimental observations demonstrate that the enhancement of air supply due to the chimney effect must facilitate UCF. It indicates that the fire risk and the environmental hazard of deep UCF may be underestimated by the conventional perception. It suggests that more rigorous fire-fighting techniques such as covering finer loess should be undertaken to effectively extinguish deep UCF.

UCF are an environmental hazard with complex hydro-thermo-chemical-mechanical (HTCM) processes in fractured porous media. Airflow that is driven by UCF generated buoyancy in turn feeds UCF itself (Ide and Orr Jr., 2011; Krevor et al., 2011); subsidence or collapse induced by UCF creates ventilation channels (Ide et al., 2010; Kuenzer and Stracher, 2012). The current work is restrained to the couplings of hydro-thermo-chemical (HTC) processes. However, mechanical mechanism controlling permeability of the ventilation channels plays an important role in the chimney effect of UCF. Unfortunately, the relationship between the ventilation channels' permeability and depth is still uncertain. The permeability may decrease with increasing the fire depth because of the thicker overburden rock strata; on the other hand, previous work reported that it could be enhanced by thermally induced mechanical failure of overburden rock layers (Buhrow, 2004).

Wind, atmospheric pressure fluctuations (Song et al., 2015b; Wessling, 2007) and topographic effect (Song et al., 2014; Song et al., 2015b) may drive air convection through ventilation channels to feed UCF. These natural forces serve as external driving sources of air supply, and their effect usually decays with increasing depth. It is expected that UCF should cease within a limited burning period while reaching a certain fire depth, if air supply is driven by these external driving forces. The fundamental cause of persistent UCF burning hundreds or even thousands of years has still not been fully understood. The present research demonstrates that the chimney effect of UCF enhances air supply with increasing the fire depth, opposite to external natural driving forces. In addition, the chimney effect of UCF is a self-sustaining, stable mechanism, unlike temporal-spatial variations of external natural driving forces. Therefore, the chimney effect is a significant mechanism for the persistence of UCF.

5. Conclusions

The chimney effect of smoldering fire in a U-shaped porous channel, representing a simple scenario of UCF in the field, is examined in this paper. With increasing the fire depth, air flow dragged by buoyant smoke generated by UCF increases, and the burning rate, the fire spread rate, as well as the burning temperature of UCF are facilitated. Both air flow and burning status are associated with the permeability of porous media in the channel. At an extremely harsh condition like percolation channel, the chimney effect may be switched off when the permeability of the channel is less than the critical level such as 10^{-7} m^2.

Air supply is a key factor for the persistency of UCF. With the external natural driving forces such as wind, topographic effect and atmospheric pressure fluctuation, it is expected that air supply to UCF should decay with increasing the fire depth. At this circumstance, UCF will be extinct within a limited time period when it reaches a certain fire depth. However, the chimney effect induced by UCF itself may enhance air supply and facilitate coal burning with increasing fire depth, which allows UCF burning towards deeper coal seam for a long-term period until coal reservoir is completely consumed. Therefore, the chimney effect induced by smoldering fire in a U-shaped porous channel is a significant governing mechanism for the persistency of UCF.

Acknowledgements:

References

Auletta, A., Manca, O., Musto, M., Nardini, S., 2003. Thermal design of symmetrically and asymmetrically heated channel–chimney systems in natural convection. Appl. Therm. Eng. 23, 605-621.

Buhrow, C., Lippmann, G., Stöttner, M.T., 2004. Kohlebrände in der Volsrepublik China. Glückauf 140, 488-494.

Chen, Z., Chen, X., Zheng, Y., Sun, J., Chen, F., Shi, L., Li, F., Dong, Y., Zhang, Z., 2017. Air ingress analysis of chimney effect in the 200MWe pebble-bed modular high temperature gas-cooled reactor. Ann. Nucl. Energy 106, 143-153.

Ellyett, C.D., Fleming, A.W., 1974. Thermal infrared imagery of The Burning Mountain coal fire. Remote Sens. Environ. 3, 79-86.

Engle, M.A., Radke, L.F., Heffern, E.L., O'Keefe, J.M., Hower, J.C., Smeltzer, C.D., Hower, J.M., Olea, R.A., Eatwell, R.J., Blake, D.R., 2012. Gas emissions, minerals, and tars associated with three coal fires, Powder River Basin, USA. Sci. Total Environ. 420, 146-159.

Engle, M.A., Radke, L.F., Heffern, E.L., O'Keefe, J.M., Smeltzer, C.D., Hower, J.C., Hower, J.M., Prakash, A., Kolker, A., Eatwell, R.J., 2011. Quantifying greenhouse gas emissions from coal fires using airborne and ground-based methods. Int. J. Coal Geol. 88, 147-151.

Ganot, Y., Dragila, M.I., Weisbrod, N., 2014. Impact of thermal convection on CO 2 flux across the earth–atmosphere boundary in high-permeability soils. Agric. For. Meteorol. 184, 12-24.

Gao, Z., Yuan, X., Ji, J., Li, Y., Yang, L., 2017. Influence of stack effect on flame shapes of gas burner fires. Appl. Therm. Eng. 127, 1574-1581.

Grapes, R., Zhang, K., Peng, Z.L., 2009. Paralava and clinker products of coal combustion, Yellow River, Shanxi Province, China. Lithos 113, 831-843.

Hadden, R., Rein, G., 2011. Burning and water suppression of smoldering coal fires in small-scale laboratory experiments, in: Stracher, G.B., Prakash, A., Sokol, E.V. (Eds.), Coal and Peat Fires: A Global Perspective. Elsevier, Boston, pp. 318-326.

Hower, J.C., Henke, K., O'Keefe, J.M.K., Engle, M.A., Blake, D.R., Stracher, G.B., 2009. The Tiptop coal-mine fire, Kentucky: preliminary investigation of the measurement of mercury and other hazardous gases from coal-fire gas vents. Int. J. Coal Geol. 80, 63-67.

Huang, J., Bruining, J., Wolf, K.-H., 2001. Modeling of gas flow and temperature fields in underground coal fires. Fire Safety J. 36, 477-489.

Huang, X., Rein, G., 2017. Downward spread of smouldering peat fire: the role of moisture, density and oxygen supply. Int. J. Wildland Fire 26, 907-918.

Ide, S.T., Orr Jr., F.M., 2011. Comparison of methods to estimate the rate of CO2 emissions and coal consumption from a coal fire near Durango, CO. Int. J. Coal Geol. 86, 95-107.

Ide, T.S., Pollard, D., Orr Jr, F.M., 2010. Fissure formation and subsurface subsidence in a coalbed fire. Int. J. Rock Mech. Min. Sci.   47, 81-93.

Ji, J., Li, M., Shi, W., Gao, Z., Sun, J., Lo, S., 2017. Deflection characteristic of flame with the airflow induced by stack effect. Int. J. Therm. Sci. 115, 160-168.

Jiang, L., Lin, H., Ma, J., Kong, B., Wang, Y., 2011. Potential of small-baseline SAR interferometry for monitoring land subsidence related to underground coal fires: Wuda (Northern China) case study. Remote

Sens. Environ. 115, 257-268.

Krevor, S.C.M., Ide, T., Benson, S.M., Franklin M. Orr, J., 2011. Real-time tracking of CO_2 injected into a subsurface coal fire through high-frequency measurements of the $^{13}CO_2$ signature. Environ. Sci. Technol. 45, 4176-4186.

Kuenzer, C., Stracher, G.B., 2012. Geomorphology of coal seam fires. Geomorphology 138, 209-222.

Kuenzer, C., Zhang, J., Sun, Y., Jia, Y., Dech, S., 2012. Coal fires revisited: The Wuda coal field in the aftermath of extensive coal fire research and accelerating extinguishing activities. Int. J. Coal Geol. 102, 75-86.

Kuenzer, C., Zhang, J., Tetzlaff, A., van Dijk, P., Voigt, S., Mehl, H., Wagner, W., 2007. Uncontrolled coal fires and their enviornmental impacts: Investigating two arid mining regions in north-central China. Appl. Geogr. 27, 42-62.

Lei, Y., Zhang, Y., Wang, F., Wang, X., 2016. Enhancement of natural ventilation of a novel roof solar chimney with perforated absorber plate for building energy conservation. Appl. Therm. Eng. 107, 653-661.

Li, J., Fu, P., Zhu, Q., Mao, Y., Yang, C., 2018. A lab-scale experiment on low-temperature coal oxidation in context of underground coal fires. Appl. Therm. Eng. 141, 333-338.

Linden, P.F., 2003. The fluid mechanics of natural ventilation. Annu. Rev. Fluid Mech. 31, 309-335.

Liu, S., Wang, C., Zhang, S., Liang, J., Chen, F., Zhao, K., 2012. Formation and distribution of polycyclic aromatic hydrocarbons (PAHs) derived from coal seam combustion: A case study of the Ulanqab lignite from Inner Mongolia, northern China. Int. J. Coal Geol. 90, 126-134.

Liu, W., Qin, Y., Shi, C., Guo, D., 2019. Dynamic evolution of spontaneous combustion of coal in longwall gobs during mining-stopped period. Process. Saf. Environ. Prot. 132, 11-21.

Liu, Y., Xiao, Y., Augenbroe, G., Zhou, T., Hu, Y., Lin, J., Huang, H., 2018. The formation of multi-steady-states of buoyancy ventilation in underground building. Tunn. Undergr. Sp. Tech. 82, 613-626.

Lu, X., Zhu, H., Wang, D., Hu, C., Zhao, H., Huo, Y., 2018. Flow characteristic investigation of inhibition foam used for fire extinguishment in the underground goaf. Process. Saf. Environ. Prot. 116, 159-168.

Nasri, Z., Laatar, A.H., Balti, J., 2015. Natural convection enhancement in an asymmetrically heated channel-chimney system. Int. J. Therm. Sci. 90, 122-134.

O'Keefe, J.M., Henke, K.R., Hower, J.C., Engle, M.A., Stracher, G.B., Stucker, J., Drew, J.W., Staggs, W.D., Murray, T.M., Hammond III, M.L., 2010. CO_2, CO, and Hg emissions from the Truman Shepherd and Ruth Mullins coal fires, eastern Kentucky, USA. Sci. Total Environ. 408, 1628-1633.

Pironi, P., Switzer, C., Gerhard, J.I., Rein, G., Torero, J.L., 2011. Self-sustaining smoldering combustion for NAPL remediation: laboratory evaluation of process sensitivity to key parameters. Environ. Sci. Technol. 45, 2980-2986.

Pironi, P., Switzer, C., Rein, G., Fuentes, A., Gerhard, J.I., Torero, J.L., 2009. Small-scale forward smouldering experiments for remediation of coal tar in inert media. Proc. Combust. Inst. 32, 1957-1964.

Prakash, A., Schaefer, K., Witte, W.K., Collins, K., Gens, R., Goyette, M.P., 2011. A remote sensing and GIS based investigation of a Boreal Forest Coal Fire. Int. J. Coal Geol. 86, 79-86.

Rein, G., 2013. Smouldering Fires and Natural Fuels. In: Belcher, C. (Ed.), Fire Phenomena and the Earth System: An Interdisciplinary Guide to Fire Science. Wiley and Sons, pp. 15-34.

Sharma, R.P., Makinde, O.D., Animasaun, I.L., 2018. Buoyancy effects on MHD unsteady convection of a radiating chemically reacting fluid past a moving porous vertical plate in a binary mixture. Defect Diffus. Forum 387, 308-318.

Shi, B., Su, H., Li, J., Qi, H., Zhou, F., Torero, J.L., Chen, Z., 2017. Clean power generation from the intractable natural coalfield fires: Turn harm into benefit. Sci. Rep.-UK 7, 5302.

Shi, W.X., Ji, J., Sun, J.H., Lo, S.M., Li, L.J., Yuan, X.Y., 2014. Influence of staircase ventilation state on the airflow and heat transfer of the heated room on the middle floor of high rise building. Appl. Energ. 119, 173-180.

Simmons, W.B., Cosca, M.A., Essene, E.J., Geissman, J.W., Coates, D.A., 1989. Pyrometamorphic rocks associated with naturally burned coal beds, Powder River Basin, Wyoming. Am. Mineral. 74, 85-100.

Singh, A.K., Singh, R.V.K., Singh, M.P., Chandra, H., Shukla, N.K., 2007. Mine fire gas indices and their application to Indian underground coal mine fires. Int. J. Coal Geol. 69, 192-204.

Song, Z., Fan, H., Jiang, J., Li, C., 2017a. Insight into effects of pore diffusion on smoldering kinetics of coal using a 4-step chemical reaction model. J. Loss Prevent. Proc. 48, 312-319.

Song, Z., Huang, X., Jiang, J., Pan, X., 2019a. A laboratory approach to CO_2 and CO emission factors from underground coal fires. Int. J. Coal Geol., Minor revision.

Song, Z., Huang, X., Luo, M., Gong, J., Pan, X., 2017b. Experimental study on the diffusion–kinetics interaction in heterogeneous reaction of coal. J. Therm. Anal. Calorim. 127, 1625–1637.

Song, Z., Kuenzer, C., 2014. Coal fires in China over the last decade: A comprehensive review. Int. J. Coal Geol. 133, 72-99.

Song, Z., Kuenzer, C., Zhu, H., Zhang, Z., Jia, Y., Sun, Y., Zhang, J., 2015a. Analysis of coal fire dynamics in the Wuda syncline impacted by fire-fighting activities based on in-situ observations and Landsat-8 remote sensing data. Int. J. Coal Geol. 141-142, 91-102.

Song, Z., Wu, D., Jiang, J., Pan, X., 2019b. Thermo-solutal buoyancy driven air flow through thermally decomposed thin porous media in a U-shaped channel: Towards understanding persistent underground coal fires. Appl. Therm. Eng. 159, 113948.

Song, Z., Zhu, H., Tan, B., Wang, H., Qin, X., 2014. Numerical study on effects of air leakages from abandoned galleries on hill-side coal fires. Fire Safety J. 69, 99-110.

Song, Z., Zhu, H., Xu, J., Qin, X., 2015b. Effects of atmospheric pressure fluctuations on hill-side coal fires and surface anomalies. Int. J. Min. Sci. Technol. 25, 1037-1044.

Tang, Y., Si, S., Zhong, X., 2019. Experimental investigation of the performance of an effective self-suctioning water mist generator for controlling underground coal fires. Process. Saf. Environ. Prot. 126, 98-105.

van Dijk, P., Zhang, J., Jun, W., Kuenzer, C., Wolf, K.-H., 2011. Assessment of the contribution of in-situ combustion of coal to greenhouse gas emission; based on a comparison of Chinese mining information to previous remote sensing estimates. Int. J. Coal Geol. 86, 108-119.

Wang, C., Yang, S., Li, X., 2018. Simulation of the hazard arising from the coupling of gas explosions and spontaneously combustible coal due to the gas drainage of a gob. Process. Saf. Environ. Prot. 118, 296-306.

Wang, S., Li, X., Wang, D., 2016. Mining-induced void distribution and application in the hydro-thermal investigation and control of an underground coal fire: A case study. Process. Saf. Environ. Prot. 102, 734-756.

Wessling, S., 2007. The Investigation of Underground coal fires - Towards A Numerical Approach for Thermally, Hydraulically, and Chemically Coupled Processes. Westfälische Wilhelms-University of Muenster, Germany (PhD Thesis).

Wessling, S., Kessels, W., Schmidt, M., Krause, U., 2008a. Investigating dynamic underground coal fires by means of numerical simulation. Geophys. J. Int. 172, 439-454.

Wessling, S., Kuenzer, C., Kessels, W., Wuttke, M.W., 2008b. Numerical modeling for analyzing thermal surface anomalies induced by underground coal fires. Int. J. Coal Geol. 74, 175-184.

Wolf, K.-H., Bruining, H., 2007. Modelling the interaction between underground coal fires and their roof rocks. Fuel 86, 2761-2777.

Yan, Y., Peng, L., Cheng, N., Bai, H., Mu, L., 2015. Health risk assessment of toxic VOCs species for the coal fire well drillers. Environ. Sci. Pollut. Res. 22, 15132-15144.

Yang, F., Qiu, D., 2019. Exploring coal spontaneous combustion by bibliometric analysis. Process. Saf. Environ. Prot. 132, 1-10.

Yang, J., Chen, H., 2018. Natural downward smouldering of peat: Effects of inorganic content and piled bed height. Fire Technol. 1-29.

Yokelson, R.J., Griffith, D.W.T., Ward, D.E., 1996. Open‐path Fourier transform infrared studies of large‐scale laboratory biomass fires. J. Geophys. Res. Atmos. 101, 21067.

Zamora, B., Kaiser, A.S., 2009. Optimum wall-to-wall spacing in solar chimney shaped channels in natural convection by numerical investigation. Appl. Therm. Eng. 29, 762-769.

Zhang, J., Kuenzer, C., 2007. Thermal surface characteristics of coal fires 1: results of in-situ measurements. J. Appl. Geophys. 63, 117-134.

Zhou, X., Yang, J., Xiao, B., Hou, G., Xing, F., 2009. Analysis of chimney height for solar chimney power plant. Appl. Therm. Eng. 29, 178-185.

Zhuo, H., Qin, B., Qin, Q., Su, Z., 2019. Modeling and simulation of coal spontaneous combustion in a gob of shallow buried coal seams. Process. Saf. Environ. Prot. 131, 246-254.